**Supplemental Figures**

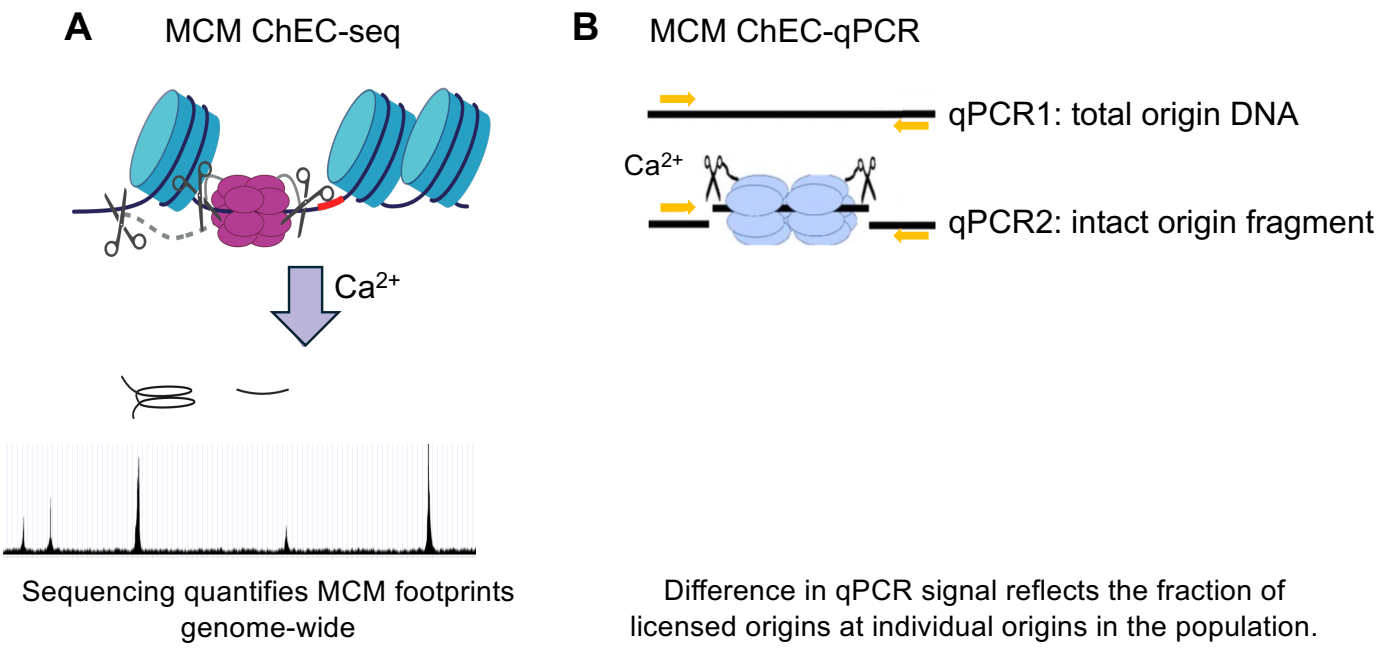


**Figure S1. Principle of the MCM–ChEC assays used to measure origin licensing.**

(A) MCM–ChEC-seq. Micrococcal nuclease (MNase) fused to an MCM subunit cleaves DNA adjacent to loaded MCM double hexamers upon addition of $Ca^{2+}$. Sequencing of the resulting fragments quantifies MCM footprints genome-wide, providing a measure of helicase loading at replication origins. Libraries were prepared without size selection, ensuring retention of small MNase fragments; larger fragments are disfavored during library preparation due to their size.

(B) MCM–ChEC-qPCR. MNase cleavage at licensed origins disrupts the PCR amplicon spanning the cleavage site. Quantitative PCR using origin-specific primers amplifies only intact origin DNA; cleavage therefore reduces the qPCR signal in proportion to the fraction of origins that have undergone MNase cleavage. Because MNase cleavage occurs only at origins that have loaded an MCM double hexamer, the decrease in qPCR signal provides a quantitative measure of the fraction of licensed origins in the population.

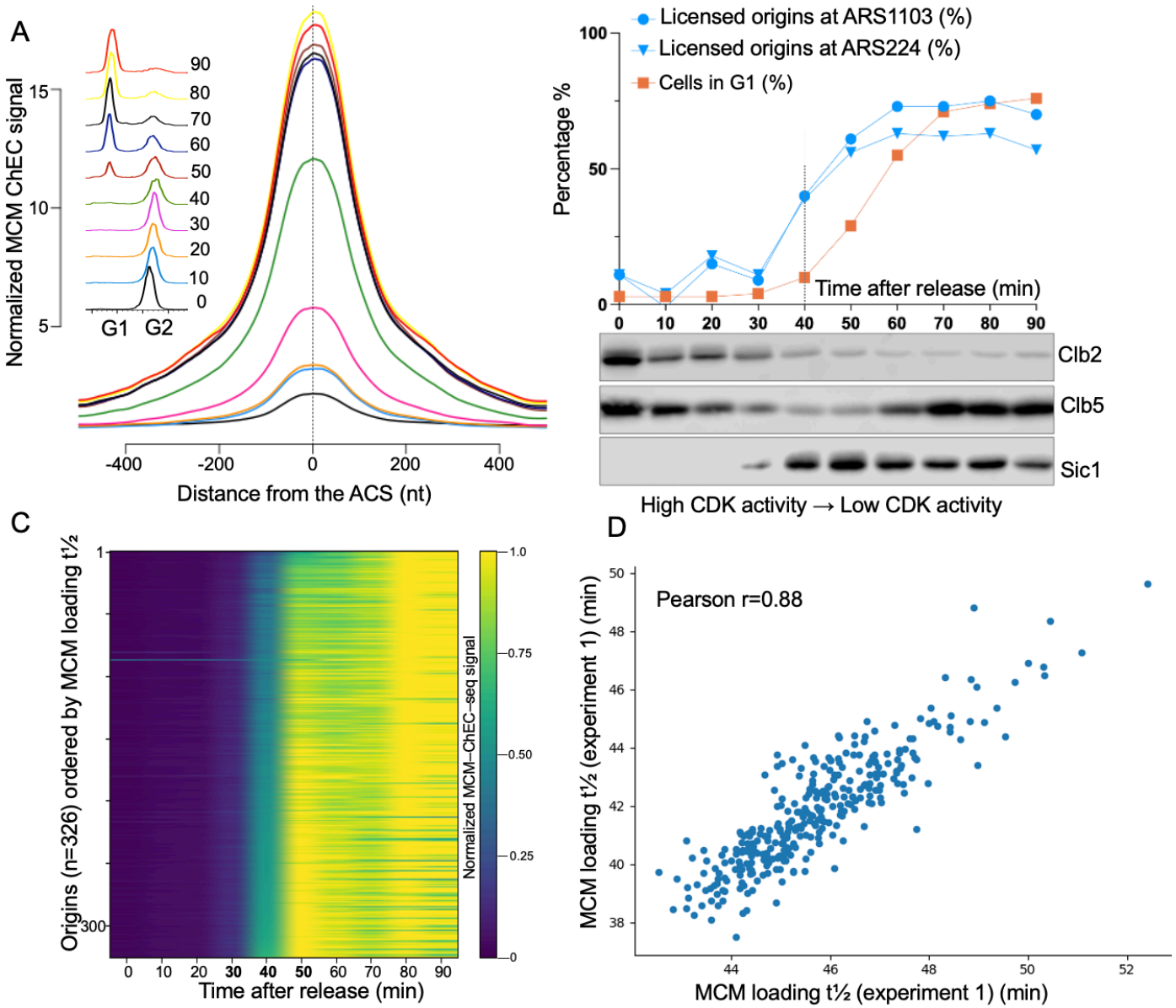


**Figure S2. Independent replicate of the replication origin licensing time course.**

(A) Aggregate MCM–ChEC–seq signal across origins following release from nocodazole arrest. Normalized MCM–ChEC signal averaged across 326 annotated replication origins and aligned relative to the ACS is shown for the indicated times after release. As observed in the experiment shown in Figure 1, MCM signal is low in G2/M and increases sharply within ~20–40 min after release, reaching near-maximal levels by ~50–60 min. Insets show representative DNA-content profiles corresponding to each time point.

(B) Quantification of licensing and CDK regulatory markers during the same time course. The fraction of licensed origins at two origins (ARS1103 and ARS224) was measured by ChEC–qPCR (blue) and compared with the fraction of cells in G1 determined by flow cytometry (orange). Immunoblot analysis of Clb2 and Clb5 together with the CDK inhibitor Sic1 shows rapid loss of B-type cyclins and accumulation of Sic1 coincident with the onset of MCM loading, consistent with licensing occurring as CDK activity declines. qPCR results are available in Supplemental Table S5.

(C) Genome-wide kinetics of helicase loading. Heatmap of normalized MCM–ChEC–seq signal across 326 origins, aligned relative to the ACS as in (A) and ordered by the time to half-maximal MCM loading (t½). As in Figure 1, most origins acquire MCM signal within the same narrow time window, demonstrating highly synchronous genome-wide helicase loading. MCM-ChEC signal and t½ values for individual origins are provided in Supplemental Table S4.

(D) Reproducibility of origin-specific licensing kinetics. Comparison of the time to half-maximal MCM loading (t½) for each origin between two independent experiments. Each point represents one origin (n = 326). The strong correlation (Pearson r = 0.88) indicates that origin-specific licensing kinetics are highly reproducible despite a modest offset in absolute timing between experiments.

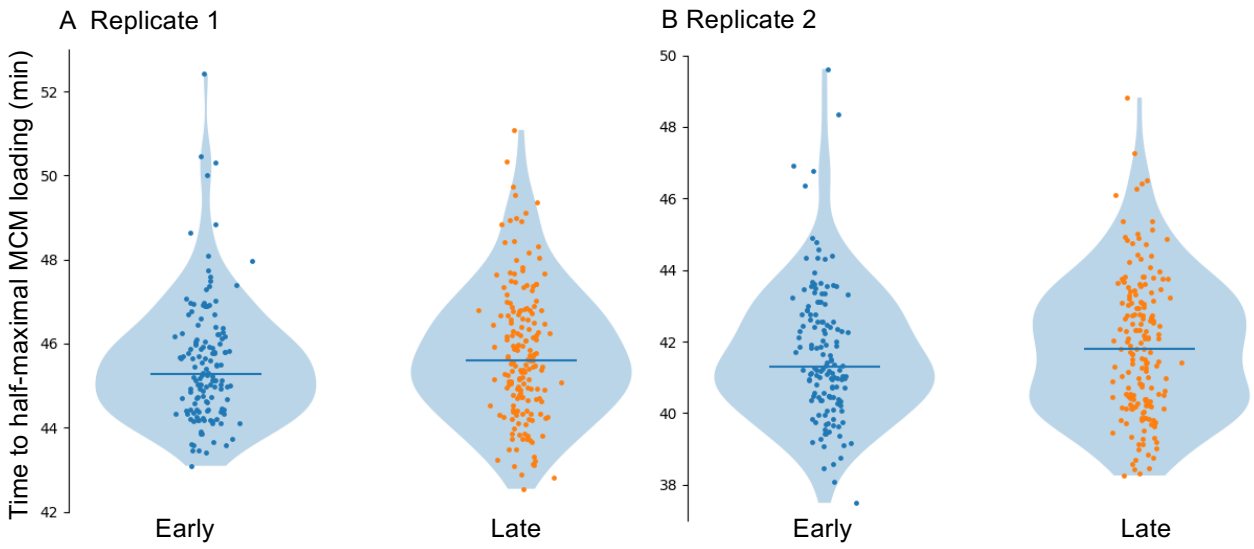


**Figure S3. Early- and late-replicating origins exhibit similar licensing kinetics.**

(A) Distribution of the time to half-maximal MCM loading (t½) for origins previously classified as early- or late-replicating in the experiment shown in Figure 1. Each point represents one origin, and violin plots show the distribution of t½ values within each class. Horizontal lines indicate the mean. Classification of early and late origins and t½ values for individual origins are provided in Supplemental Table S4.

(B) Same analysis as in (A) for the independent replicate experiment shown in Figure S2. Early- and late-replicating origins exhibit largely overlapping distributions of licensing kinetics in both experiments, indicating that replication timing classes do not differ substantially in the timing of MCM loading.

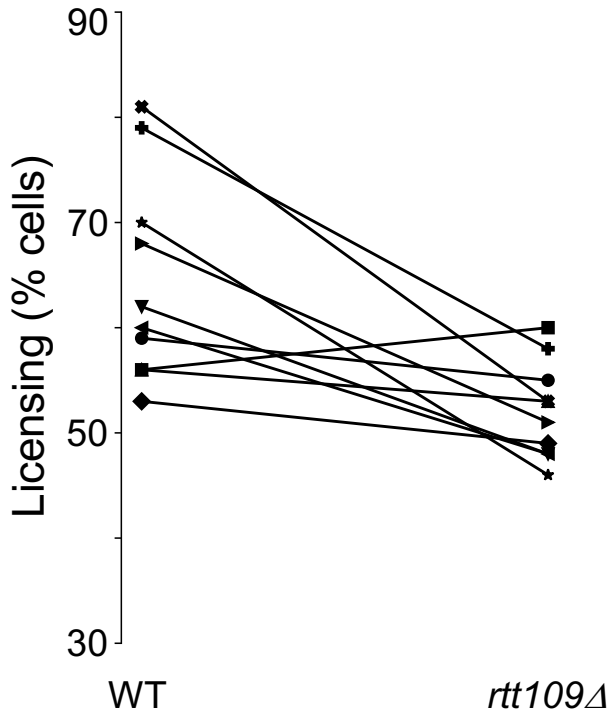


**Figure S4. Independent replicate confirming reduced origin licensing in *rtt109*Δ cells.**

MCM loading was measured by ChEC–qPCR at ten replication origins in wild-type and *rtt109*Δ cells in an independent experiment. As observed in Figure 2A, loss of H3K56 acetylation in *rtt109*Δ cells caused a modest but reproducible reduction in licensing relative to wild type (mean −19%; range −35% to +7%; paired two-tailed t-test p = 0.0046). Each line represents an individual origin. Individual qPCR values are provided in Supplemental Table S8.

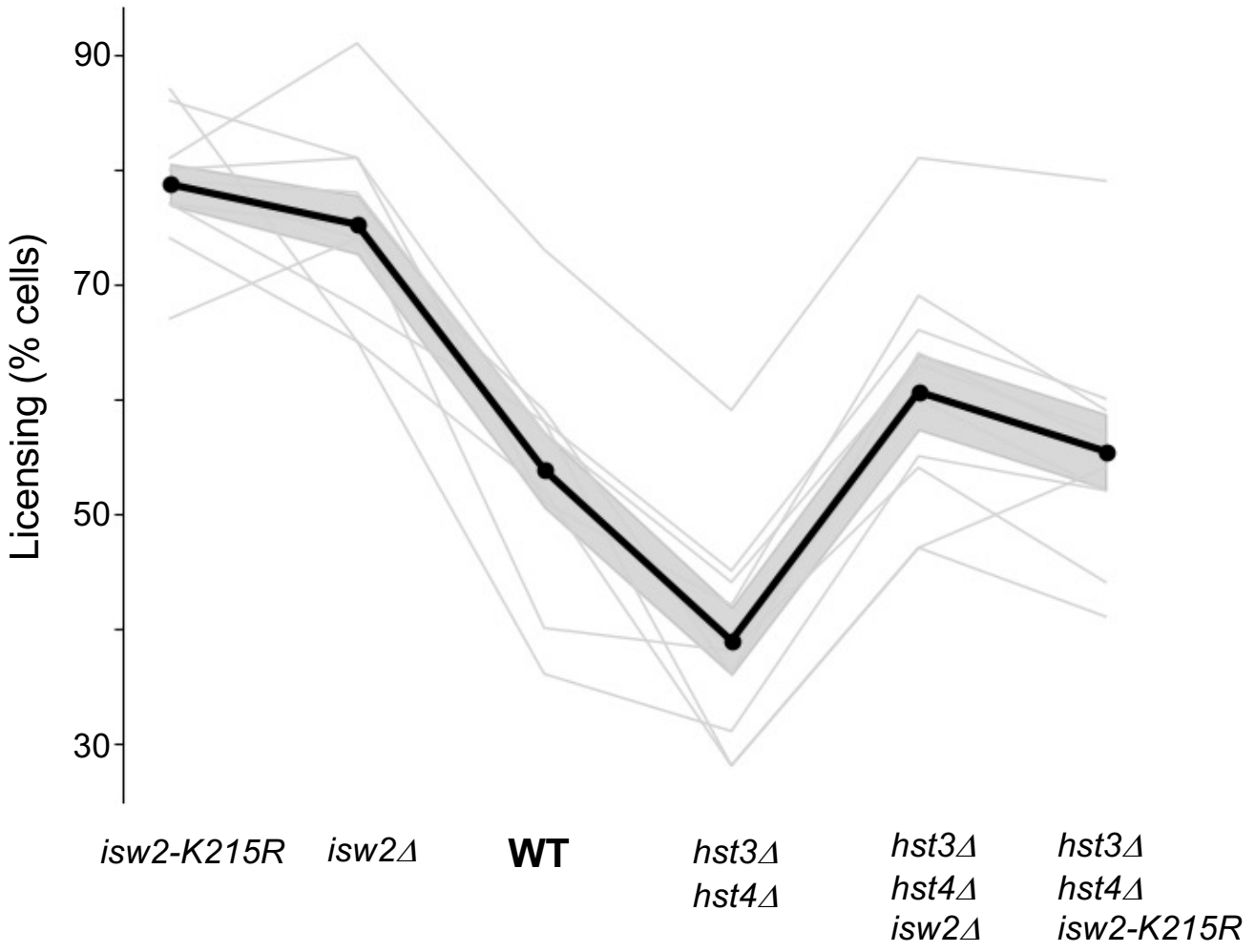


**Figure S5. Independent biological replicate of the experiment shown in Figure 2D.**

MCM loading was measured by ChEC–qPCR at ten replication origins in the indicated strains in an independent biological replicate. The same pattern observed in Figure 2 was reproduced: deletion of *ISW2* increased licensing relative to wild type, whereas *hst3*Δ *hst4*Δ cells exhibited a pronounced licensing defect that was strongly suppressed by deletion of *ISW2*. The ATPase-dead *isw2*-K215R allele phenocopied *isw2*Δ in both wild-type and *hst3*Δ *hst4*Δ backgrounds, indicating that catalytic remodeling activity of Isw2 is required for inhibition of origin licensing. Thin gray lines represent individual origins; the thick black line indicates the mean across origins, and the shaded region denotes ± SEM. Individual qPCR values are provided in Supplemental Table S6.

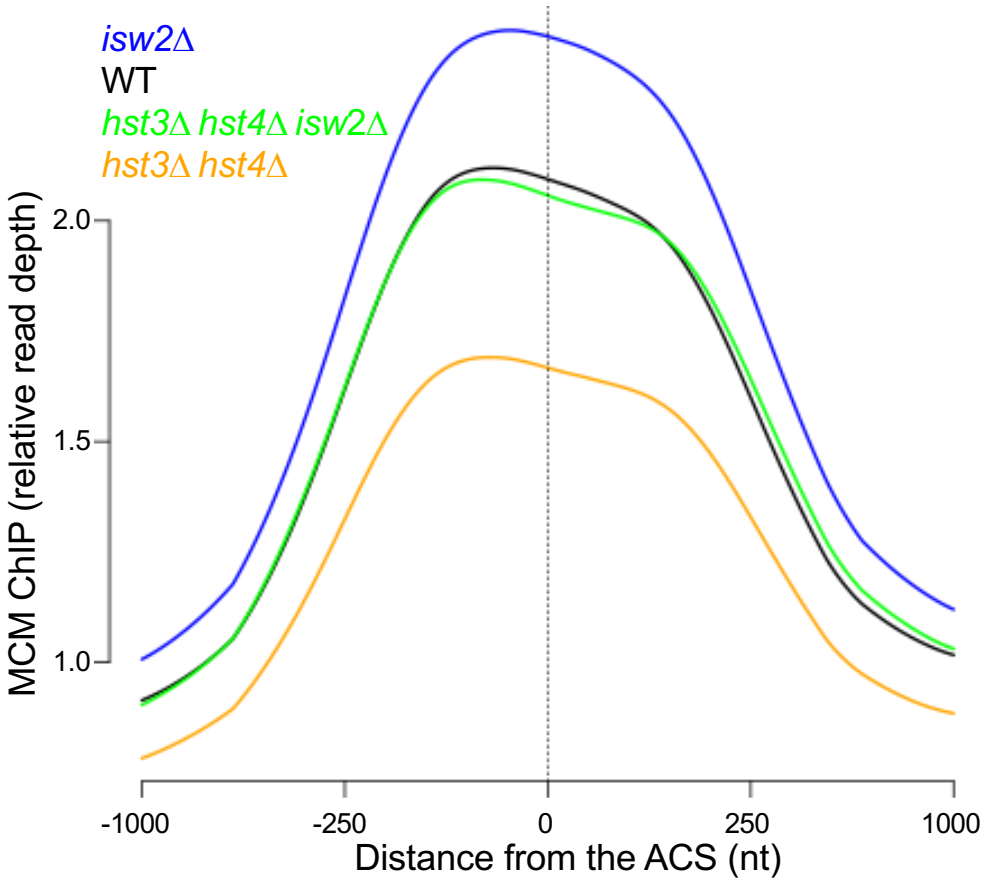


**Figure S6. Genome-wide MCM ChIP confirms licensing differences across genotypes.**

Average MCM ChIP signal across 326 replication origins aligned relative to the ARS consensus sequence (ACS) in the indicated genotypes (WT, *isw2*Δ, *hst3*Δ *hst4*Δ, and *isw2*Δ *hst3*Δ *hst4*Δ). Origin-associated MCM signal is reduced in *hst3*Δ *hst4*Δ, increased in *isw2*Δ, and restored in *isw2*Δ *hst3*Δ *hst4*Δ, consistent with the licensing differences measured by MCM–ChEC. An independent biological replicate yielded highly similar results; the corresponding values for both replicates are provided in Supplemental Table S11.

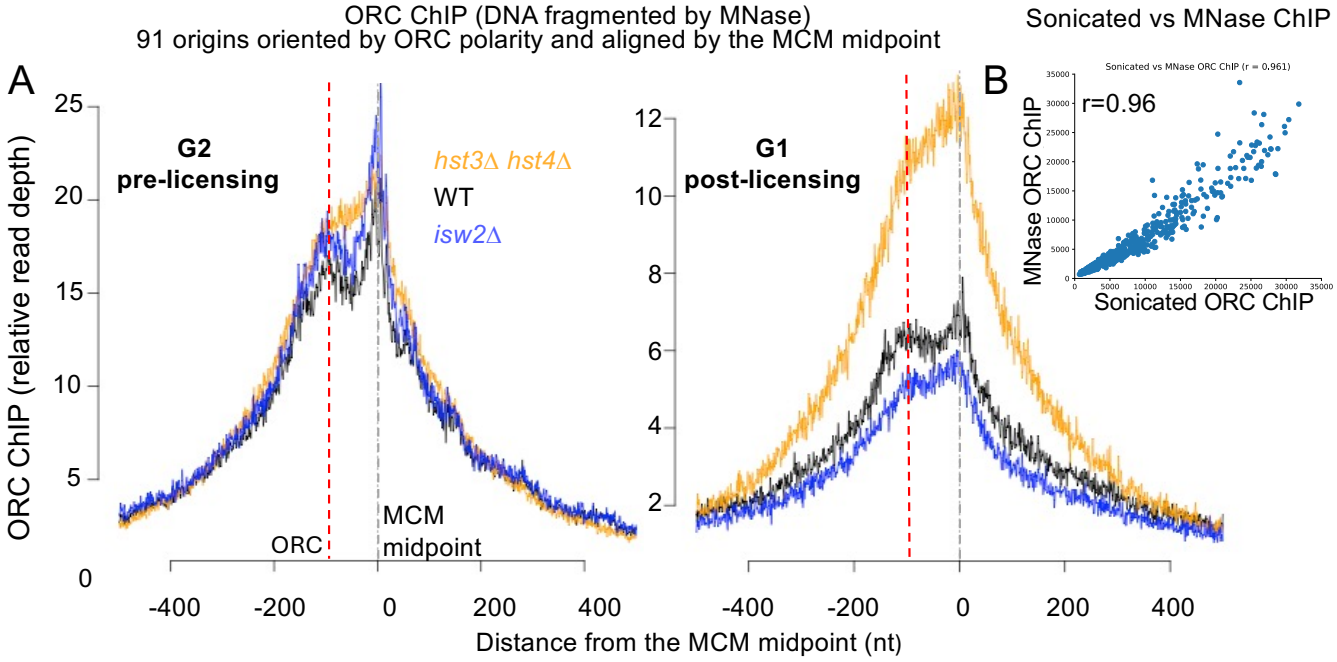


**Figure S7. ORC ChIP profiles using MNase-fragmented chromatin**

(A) Average ORC ChIP signal across 91 replication origins oriented by ORC polarity and aligned by the MCM loading midpoint in G2/M (pre-licensing) and G1 (post-licensing) cells of the indicated genotypes (WT, *isw2*Δ, and *hst3*Δ *hst4*Δ). Chromatin was fragmented using exogenous MNase digestion. As in the sonicated ChIP experiment shown in Figure 3, the ORC peak lies to the left of the MCM midpoint, consistent with the orientation of the curated origin set. Although the contours of the profiles differ from those obtained with sonicated chromatin, reflecting differences in fragmentation, the relative ORC occupancy patterns across genotypes are preserved. Relative ORC ChIP signal at each of the 91 origins for both fragmentation methods is provided in Supplemental Table S10.

(B) Correlation between ORC ChIP signals obtained from sonicated and MNase-fragmented chromatin across all origins and conditions (Pearson $r = 0.96$, $N = 546$), demonstrating strong agreement between the two fragmentation methods.

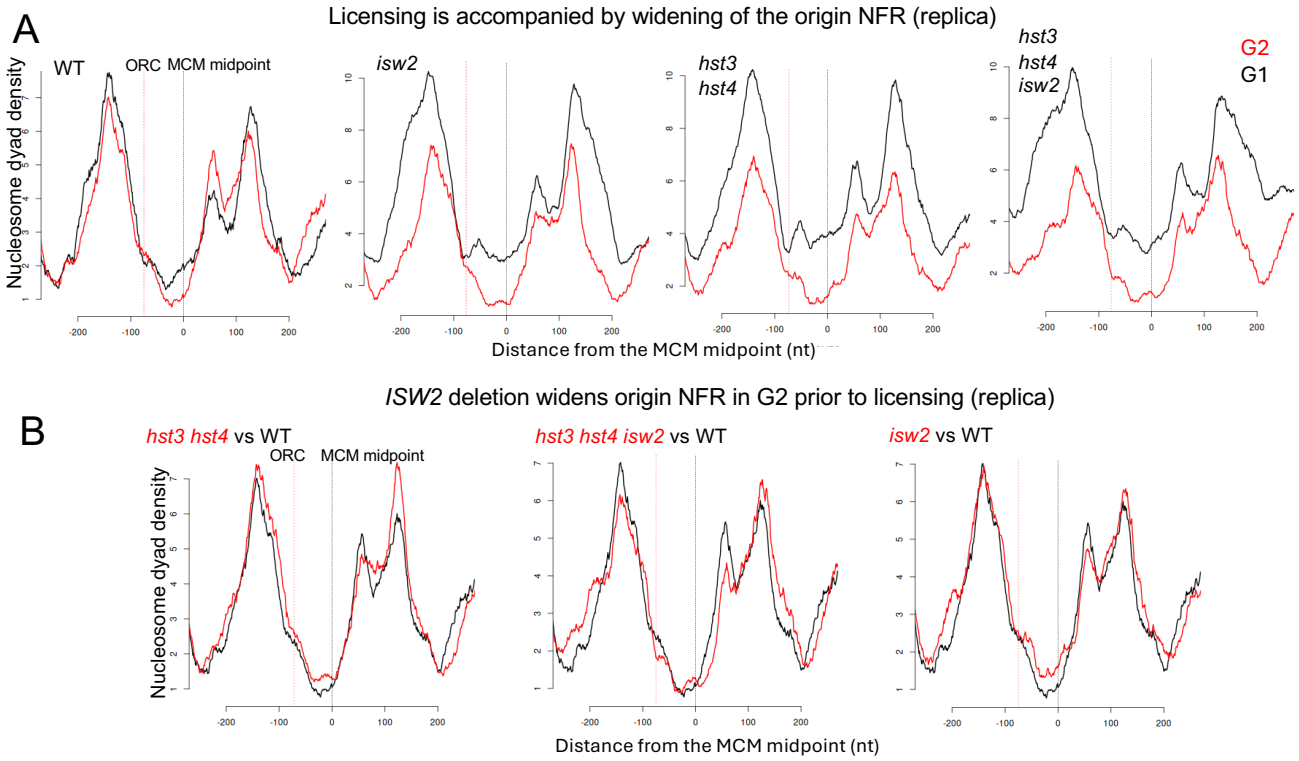


**Figure S8. Independent biological replicate of nucleosome mapping at replication origins.**

(A) Nucleosome dyad density profiles derived from MNase digestion in G2/M (red) and G1 (black) cells for the indicated genotypes across 91 oriented replication origins. Profiles are aligned to the MCM midpoint and oriented as in Figures 3–5. Vertical dashed lines indicate the ORC binding site and the MCM midpoint. As in Figure 5A, licensing in wild-type cells is accompanied by outward repositioning of nucleosomes flanking the origin NDR during G1.

(B) Direct comparison of nucleosome organization in G2/M prior to licensing. As in Figure 5B, deletion of *ISW2* widens the origin NDR and repositions flanking nucleosomes outward in the *hst3*Δ *hst4*Δ background. These results reproduce the nucleosome architecture changes observed in Figure 5.

## Supplemental Tables

### Supplemental Table S1. Yeast strains used in this study

| Strain ID | Genotype | Source |
|---|---|---|
| 16652 | MATa his3 leu2 ura3 met15 | This study |
| 16964 | MATa his3 leu2 ura3 met15 hmlαΔ::NAT MCM2-3xFLAG-MNase::KanMX | This study |
| 16991 | GP2 h− (L972) wild-type *Schizosaccharomyces pombe* | Gift from G. Smith |
| 17000 | GP2 h− (L972) MCM2-3xFLAG-MNase::KanMX | This study |
| 17862 | MATa his3 leu2 ura3 met15 hmlαΔ::NAT MCM2-3xFLAG-MNase::KanMX isw2Δ::Hyg | This study |
| 17868 | MATa his3 leu2 ura3 met15 hmlαΔ::NAT MCM2-3xFLAG-MNase::KanMX isw1Δ::Hyg | This study |
| 17870 | MATa his3 leu2 ura3 met15 hmlαΔ::NAT MCM2-3xFLAG-MNase::KanMX chd1Δ::Hyg | This study |
| 17876 | MATa his3 leu2 ura3 met15 hmlαΔ::NAT MCM2-3xFLAG-MNase::KanMX nhp10Δ::Hyg | This study |
| 17878 | MATa his3 leu2 ura3 met15 hmlαΔ::NAT MCM2-3xFLAG-MNase::KanMX rtt109Δ::Hyg | This study |
| 17887 | MATa his3 leu2 ura3 met15 hmlαΔ::NAT MCM2-3xFLAG-MNase::KanMX hst4Δ::Hyg hst3Δ::LEU2 | This study |
| 17913 | MATa his3 leu2 ura3 met15 isw2Δ::Hyg | This study |
| 17923 | MATa his3 leu2 ura3 met15 hmlαΔ::NAT MCM2-3xFLAG-MNase::KanMX hst4Δ::Hyg hst3Δ::LEU2 isw2Δ::URA3 | This study |
| 17941 | MATa his3 leu2 ura3 met15 hst4Δ::Hyg hst3Δ::LEU2 isw2Δ::URA3 | This study |
| 17945 | MATa his3 leu2 ura3 met15 hst4Δ::KanMX hst3Δ::Hyg | This study |
| 17947 | MATa his3 leu2 ura3 met15 SIC1-TAP::HIS3MX6 | Open Biosystems |
| 17948 | MATa his3 leu2 ura3 met15 CLB2-TAP::HIS3MX6 | Open Biosystems |
| 17949 | MATa his3 leu2 ura3 met15 CLB5-TAP::HIS3MX6 | Open Biosystems |
| 17967 | MATa his3 leu2 ura3 met15 ORC2-6xGly-3xFLAG::KanMX | This study |
| 17976 | MATa his3 leu2 ura3 met15 ORC2-6xGly-3xFLAG::KanMX isw2Δ::HIS3 | This study |
| 17980 | MATa his3 leu2 ura3 met15 ORC2-6xGly-3xFLAG::KanMX hst3Δ::Hyg hst4Δ::NAT | This study |
| 18100 | MATa his3 leu2 ura3 met15 hmlαΔ::NAT MCM2-3xFLAG-MNase::KanMX hst4Δ::Hyg hst3Δ::LEU2 isw2-K215R | This study |
| 18103 | MATa his3 leu2 ura3 met15 hmlαΔ::NAT MCM2-3xFLAG-MNase::KanMX isw2-K215R | This study |

**Supplemental Table S2. Plasmids used in this study**

| Plasmid ID | Description | Source |
|---|---|---|
| pGZ108 | pFA6a-3FLAG-MNase-kanMX6, Addgene #70231 | Zentner et al., 2015 |
| pGZ109 | pFA6a-3FLAG-MNase-HIS3MX6, Addgene #70232 | Zentner et al., 2015 |
| pRS406-ISW2-GRT | K215R mutation in the ATPase domain of ISW2 | Gelbart et al., 2005 |

**Supplemental Table S3. Primers used for qPCR**

| Primer Name | Target | Sequence (5'→3') |
|---|---|---|
| Tor2_5P_qPCR | TOR2 | GCACAAAGACCACAAAGTCG |
| Tor2_3P_qPCR | TOR2 | GGGGATAGAGAACTAACAAAAGCA |
| ARS216_qPCR_Forward | ARS216 | CCCTTGGTATACCTTTTCTGTG |
| ARS216_qPCR_Reverse | ARS216 | CCCATCTTTAAGCTCTGCTGTG |
| ARS224_qPCR_Forward | ARS224 | GCATAATGCCTTATTTTGTACC |
| ARS224_qPCR_Reverse | ARS224 | GGCACATTCATACTTATCTTAGC |
| ARS315_qPCR_Forward | ARS315 | GTGGGTATTTCCGTGTATATGG |
| ARS315_qPCR_Reverse | ARS315 | GGTATTTGCAGTATTTTCTTGGC |
| ARS419_qPCR_Forward | ARS419 | GAGCTTTAAACAAGGAGGAG |
| ARS419_qPCR_Reverse | ARS419 | GATAACCGATGACTTGGCAAG |
| ARS605_qPCR_Forward | ARS605 | CCCAGACACAGTCTTCATTTATAC |
| ARS605_qPCR_Reverse | ARS605 | CATTCTGCAATAAAACCTGACC |
| ARS802_qPCR_Forward | ARS802 | CACTTTACACCATACAATAACCAC |
| ARS802_qPCR_Reverse | ARS802 | CTAATGTGAAGCCTGTGTAC |
| ARS1103_5P_qPCR | ARS1103 | CACTTAACTTGTTATAATTCTCCC |
| ARS1103_3P_qPCR | ARS1103 | CCATTCTGGTAGTTTTAATGTATTG |
| ARS1235_qPCR_Forward | ARS1235 | CATGGAAGGGTTACTCACAACG |
| ARS1235_qPCR_Reverse | ARS1235 | CGTATTAAACTAGATGACGAACAG |
| ARS1406_qPCR_Forward | ARS1406 | GACGCATTATACAATCCTAC |
| ARS1406_qPCR_Reverse | ARS1406 | GCCATTTTATATGTACATTCATC |
| ARS1427_qPCR_Forward | ARS1427 | CAACCACAGTGGATATTTCCC |
| ARS1427_qPCR_Reverse | ARS1427 | GCCATACGAATAAGGTGG |